Inner-shell magnetic dipole transition in Tm atoms: A candidate for optical lattice clocks

D. Sukachev[*]

P.N. Lebedev Physical Institute, 53 Leninsky prospekt, Moscow 119991, Russia;
Department of Physics, Harvard University, 17 Oxford St., Cambridge, Massachusetts 02138, USA;
and Russian Quantum Center, Business-Center "Ural", 100A Novaya St., Skolkovo, Moscow 143025, Russia

S. Fedorov

Ecole polytechnique fédérale de Lausanne, Route Cantonale, 1015 Lausanne, Switzerland

I. Tolstikhina and D. Tregubov

P.N. Lebedev Physical Institute, 53 Leninsky prospekt, Moscow 119991, Russia
and Moscow Institute of Physics and Technology, 9 Institutskiy per., Dolgoprudny, Moscow region 141700, Russia

E. Kalganova, G. Vishnyakova, A. Golovizin, and N. Kolachevsky[†]

P.N. Lebedev Physical Institute, 53 Leninsky prospekt, Moscow 119991, Russia;
Moscow Institute of Physics and Technology, 9 Institutskiy per., Dolgoprudny, Moscow region 141700, Russia;
and Russian Quantum Center, Business-Center "Ural", 100A Novaya St., Skolkovo, Moscow 143025, Russia

K. Khabarova and V. Sorokin

P.N. Lebedev Physical Institute, 53 Leninsky prospekt, Moscow 119991, Russia
and Russian Quantum Center, Business-Center "Ural", 100A Novaya St., Skolkovo, Moscow 143025, Russia

We consider a narrow magneto-dipole transition in the ^{169}Tm atom at the wavelength of 1.14 μm as a candidate for a two-dimensional-optical lattice clock. Calculating dynamic polarizabilities of the two clock levels [Xe]$4f^{13}6s^2(J = 7/2)$ and [Xe]$4f^{13}6s^2(J = 5/2)$ in the spectral range from 250 to 1200 nm, we find a "magic" wavelength for the optical lattice at 807 nm. Frequency shifts due to black-body radiation (BBR), the van der Waals interaction, the magnetic dipole-dipole interaction, and other effects which can perturb the transition frequency are calculated. The transition at 1.14 μm demonstrates low sensitivity to the BBR shift corresponding to 8×10^{-17} in fractional units at room temperature which makes it an interesting candidate for high-performance optical clocks. The total estimated frequency uncertainty is less than 5×10^{-18} in fractional units. By direct excitation of the 1.14 μm transition in Tm atoms loaded into an optical dipole trap, we set the lower limit for the lifetime of the upper clock level [Xe]$4f^{13}6s^2(J = 5/2)$ of 112 ms which corresponds to a natural spectral linewidth narrower than 1.4 Hz. The polarizability of the Tm ground state was measured by the excitation of parametric resonances in the optical dipole trap at 532 nm.

I. INTRODUCTION

Magnetic-dipole transitions between the ground state fine structure components in hollow shell lanthanides are strongly shielded from external electric fields by the closed outer $5s^2$ and $6s^2$ shells. In the solid state, these well resolved transitions, protected from intracrystal electric fields, are widely used in various active media doped by Er^{3+}, Tm^{3+}, and other ions that lase in the near-infrared and infrared spectral ranges [1,2]. Such shielding can also facilitate the use of inner-shell transitions in optical frequency metrology due to their low sensitivity to external electric fields and collisions [3].

In the early era of optical atomic clocks, the dominating systematic uncertainty was the collisional shift in a cloud of laser cooled atoms [4,5]. One could expect better performance using inner-shell transitions in lanthanides, but this study was hampered by difficulties with their laser cooling. In 1983

Aleksandrov *et al.* [6] showed that the collisional broadening of the inner-shell magnetic dipole transition in the Tm atom [Xe]$4f^{13}6s^2(J = 7/2) \rightarrow$ [Xe]$4f^{13}6s^2(J = 5/2)$, where J is the total electronic angular momentum, at the wavelength of 1.14 μm in He buffer gas is suppressed by at least 500 times compared to the outer shell transitions. It was shown later that for Tm-He collisions shielding strongly reduced the spin relaxation [7], but it does not reduce the spin relaxation rate in Tm-Tm collisions due to the anisotropic nature of the magnetic dipole-dipole interaction [8].

The problem with atom-atom collisions in optical clocks was solved after the invention of an optical lattice clock [9,10] which resulted in the rapid progress of accuracy and stability over the last decade [11]. Today, lattice clocks based on Sr [12] and Yb [13] demonstrate unprecedentedly small fractional frequency instabilities in the low 10^{-18} range.

One of the important limiting factors is the shift caused by black-body radiation (BBR) [14–16]. The optical clock community continues an intensive search for alternative candidates aiming for lower sensitivity to BBR and other shifts, simplicity of manipulation, and better accuracy [17,18].

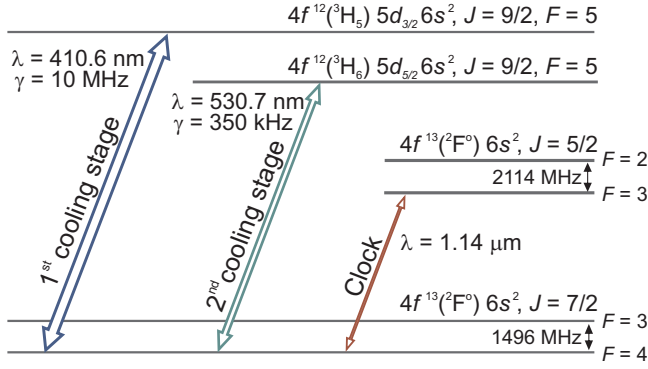[*]sukachev@gmail.com
[†]kolachbox@mail.ru

FIG. 1. Relevant energy levels of ^{169}Tm. The strong transition at 410.6 nm is used for the first-stage laser cooling and detecting the ground state populations, and the weak transition at 530.7 nm is used for the second-stage cooling. The proposed clock transition $4f^{13}6s^2(J=7/2, F=4) \rightarrow 4f^{13}6s^2(J=5/2, F=3)$ is at 1.14 μm.

Since hollow-shell lanthanides are expected to show small differential static polarizabilities of the states with different configurations of the $4f$ electrons, one expects small BBR shifts of the inner-shell magnetic dipole transitions. Taking into account large natural lifetimes of the clock levels, these transitions can be successfully used in optical lattice clocks. Recent progress in laser cooling of Er [19], Dy [20], and Tm [21,22] and frequency stabilized laser systems [23,24] open the way for experimental implementation of these ideas.

Similar to other lanthanides, laser cooling of Tm is achieved in two stages. The first cooling stage is done at the strong 410.6 nm transition which routinely produces sub-Doppler temperature of 80 μK in a cloud of 2×10^6 atoms [21]. The second cooling stage at the weak 530.7 nm transition results in the Doppler-limited temperature of 9 μK [25]. This temperature is low enough to load atoms in a shallow optical trap or a lattice using 532 nm laser radiation [22]. Relevant Tm levels are shown in Fig. 1. Further cooling of atoms is possible by optimizing the cooling sequence [26] or by evaporative cooling [27]. These experiments stimulated further study of the inner shell transition [Xe]$4f^{13}6s^2(J=7/2, F=4) \rightarrow$ [Xe]$4f^{13}6s^2(J=5/2, F=3)$, where F is the total atomic angular momentum, for its application in optical lattice clocks. In this article, the level [Xe]$4f^{13}6s^2(J=7/2)$ will be referred to as the "lower clock level" while the level [Xe]$4f^{13}6s^2(J=5/2)$ as the "upper clock level".

In the next sections, we analyze effects which may impact the performance of such clocks. First, the only stable isotope ^{169}Tm is a boson and thus the clock transition is subject to collisional shifts. The related scattering length depends on the poorly known Tm-Tm potential at small distances and is very sensitive to the calculation uncertainty of the long-range potentials [28,29]. This difficulty can be overcome if Tm atoms are loaded in a two-dimensional (2D)-optical lattice with a small filling factor canceling Tm-Tm collisions. Second, to avoid effects depending on laser intensity we calculated the dynamic polarizabilities of the upper and lower clock levels and defined a candidate for the "magic" wavelength (Sec. II). Third, the large ground-state dipole moment of Tm

atoms induces a frequency shift due to magnetic dipole-dipole interaction. Preparing Tm atoms in the $|m=0\rangle$ (here m is a magnetic quantum number) state cancels this shift but magnetic relaxation still limits the interrogation time of the clock transition and should be taken into account (Sec. III). In Sec. IV we present the error budget of the proposed Tm optical clock.

In the experimental part (Sec. V), we demonstrate direct excitation of the clock transition at 1.14 μm and measure the lifetime of the upper clock level in a one-dimensional (1D)-optical lattice formed by 532 nm laser radiation [30]. Also, we experimentally evaluate the dynamic polarizability of the Tm ground state at 532 nm by excitation of parametric resonances in the optical dipole trap.

II. POLARIZABILITIES

To find the magic wavelength and to estimate the BBR and the van der Waals shifts, one should know the energy shifts ΔE of the clock states in an external monochromatic electric field $\vec{E} = 1/2 \vec{\mathcal{E}} e^{-i\omega t} + \text{c.c.}$ at the angular frequency ω:

$$\Delta E(\omega) = -\frac{\alpha(\omega)}{4}|\mathcal{E}|^2 - \frac{\gamma(\omega)}{64}|\mathcal{E}|^4 + \cdots, \qquad (1)$$

where $\alpha(\omega)$ is the dynamic polarizability, $\gamma(\omega)$ is the hyperpolarizability, and $\vec{\mathcal{E}}$ is the complex amplitude of the electric field, both depending on m and the polarization of the field. To our knowledge, there are only a few publications where the polarizability of Tm levels was analyzed. In [31,32] the authors measured the static tensor polarizability, while a theoretical calculation of static polarizabilities without accounting for a fine-structure interaction is presented in [33]. In this section we will calculate polarizabilities of the clock states.

To suppress the site-dependent frequency shift from varying light polarization in the lattice, we suggest loading Tm atoms into a 2D-optical lattice formed by four laser beams with the same linear polarization as shown in Fig. 2. This guarantees that the trapping light polarization is the same for all lattice sites. Further in this paper, we consider only the transition $|J=7/2, F=4, m=0\rangle \rightarrow |J=5/2, F=3, m=0\rangle$ which is free from the frequency shifts induced by the magnetic dipole-
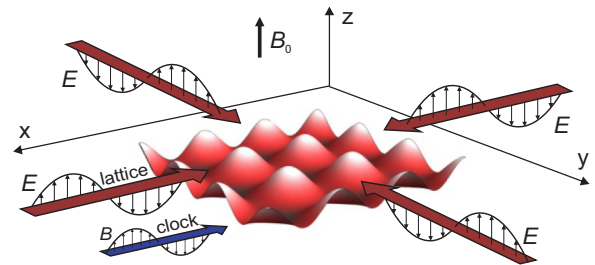

FIG. 2. Geometry of a 2D-optical lattice. The lattice is formed by four horizontal laser beams (lattice, red) with linear vertical polarization. A uniform external magnetic field B_0 is applied along the vertical axis. An interrogating laser beam (clock, blue) lies in the optical lattice plane (horizontal) to eliminate frequency shifts by the Doppler effect and photon recoil. The B component of the interrogating light should be vertical to excite the $|m=0\rangle \rightarrow |m=0\rangle$ clock transition (which is of a magnetic dipole type).

dipole interaction (see Sec. III). Since both levels have $m = 0$, the contribution from the vector polarizability for this transition also vanishes, and the total polarizability α can be separated into the scalar α^s and the tensor α^t parts [34] as follows:

$$\alpha_{JFm}(\omega) = \alpha^s_{JF}(\omega) + \alpha^t_{JF}(\omega) \frac{3m^2 - F(F+1)}{F(2F-1)},$$

$$\alpha^s_{JF}(\omega) = \frac{1}{2F+1} \sum_{m=-F}^{m=F} \alpha_{JFm}(\omega), \qquad (2)$$

$$\alpha^t_{JF}(\omega) = \alpha_{JF,m=F}(\omega) - \alpha^s_{JF}(\omega).$$

For consistency with other papers, we will calculate the polarizabilities in atomic units (a.u.); 1 a.u. $= 4\pi\epsilon_0 a_0^3 = 1.65 \times 10^{-41}$ J/(V/m)^2, where a_0 is the Bohr radius and ϵ_0 is the vacuum permittivity (for conversion to another units, see [35]).

A. Discrete spectrum

The contribution of the discrete spectrum is given by [34,36]

$$\alpha_{Fm}(\omega) = \frac{3}{2} \frac{c^3 \hbar^4}{a_0^3} \sum_{F'}' \frac{2F_u + 1}{(E_{F'} - E_F)^2} \begin{pmatrix} F_u & 1 & F_d \\ -m & 0 & m \end{pmatrix}^2$$

$$\times \frac{A_{F_u \to F_d}}{(E_{F'} - E_F)^2 - (\hbar\omega)^2}, \qquad (3)$$

where c is the speed of light, $\hbar$ is the reduced Planck's constant, and E_F and $E_{F'}$ are energies of levels $|F\rangle$ and $|F'\rangle$, respectively. The summation is over all levels F'. For each term, $F_u = F'$ and $F_d = F$ if $E_{F'} > E_F$ and vice versa. $A_{F_u \to F_d}$ is a transition probability (spontaneous decay rate) from $|F_u\rangle$ to $|F_d\rangle$.

Assuming JI coupling between the total electron momentum J and the nuclear spin I, the scalar polarizability is independent of F [34,36]:

$$\alpha^s_{JF}(\omega) = \alpha^s_J(\omega) = \frac{1}{2J+1} \sum_{m_J=-J}^{m_J=J} \alpha_{Jm_J}(\omega)$$

$$= \frac{1}{2} \frac{c^3}{a_0^3} \sum_{J'}' \frac{2J_u + 1}{2J_d + 1} \frac{1}{(\omega_{J'J})^2} \frac{A_{J_u \to J_d}}{(\omega_{J'J})^2 - \omega^2}, \qquad (4)$$

where $\omega_{J'J} = (E_{J'} - E_J)/\hbar$. The tensor polarizability equals

$$\alpha^t_{JF}(\omega) = \alpha^t_J(\omega)(-1)^{I+J+F} \begin{Bmatrix} F & J & I \\ J & F & 2 \end{Bmatrix}$$

$$\times \sqrt{\frac{F(2F-1)(2F+1)(2J+3)(2J+1)(J+1)}{(2F+3)(F+1)(2J-1)J}}, \qquad (5)$$

where

$$\alpha^t_J(\omega) = \frac{3c^3}{a_0^3} \sum_{J'}' \frac{2J_u + 1}{\omega_{J'J}^2} \frac{A_{J_u \to J_d}}{\omega_{J'J}^2 - \omega^2} (-1)^{J+J'}$$

$$\times \begin{Bmatrix} 1 & 1 & 2 \\ J_d & J_d & J_u \end{Bmatrix} \sqrt{\frac{5J(2J-1)}{6(J+1)(2J+1)(2J+3)}}. \qquad (6)$$

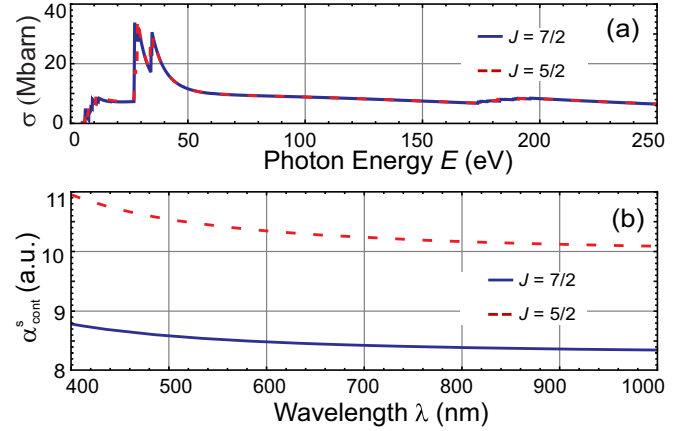Note that $\alpha^t_{7/2,4} = \alpha^t_{7/2}$ and $\alpha^t_{5/2,3} = \alpha^t_{5/2}$.

FIG. 3. (a) The photoionization cross sections for $|J = 7/2\rangle$ (solid blue) and $|J = 5/2\rangle$ (dashed red) clock levels. Peaks around 28 and 35 eV correspond to strong resonance enhancement [42]. (b) Contribution to the scalar polarizability α^s_{cont} from the continuous spectra. The hyperfine interaction is not taken into account.

As an input for the calculation of α, one should have transition probabilities $A_{J' \to J}$ from the level of interest to all others. Though many transition wavelengths in the spectral range from 250 to 807 nm and their probabilities were measured in [37,38] by Fourier-transform spectroscopy and time-resolved laser-induced fluorescence, there is still a number of transitions in the UV, visible, and IR spectral ranges which are essential for calculation and have unknown probabilities. We used the numerical package COWAN [39] to calculate transition wavelengths and probabilities in the spectral range from 250 to 1200 nm (see the Appendix).

The most self-consistent approach for calculating the differential static polarizability of the clock levels is to use only numerically calculated wavelengths and probabilities. A slight modification of this approach is used to calculate the magic wavelengths (Sec. II C).

As expected from general considerations concerning the inner shell transitions, the static scalar polarizabilities for the clock levels are nearly equal. Our calculation shows that they differ by less than 0.1 a.u. and are equal to 138 a.u. Note that the calculated static tensor polarizability of -2.7 a.u. for the lower $|J = 7/2\rangle$ clock level is in good agreement with the known experimental value of $-2.7(2)$ a.u. [31]. For the upper $|J = 5/2\rangle$ clock level our calculations give -2.3 a.u. for the tensor static polarizability.

B. Continuous spectrum

To determine the contribution of the continuous spectrum (ignoring hyperfine interaction) to the polarizability we used the formula [40]:

$$\alpha^s_{\text{cont}}(\omega) = \frac{c}{2\pi^2} \int_{\omega_I}^{\infty} \frac{\sigma(\omega')d\omega'}{(\omega' - \omega_n)^2 - \omega^2}, \qquad (7)$$

where ω_I is the photoionization limit and $\sigma(\omega)$ is the photoionization cross section of the energy level. The ionization cross section was numerically calculated using the package FAC [41] and the results are shown in Fig. 3(a). Using these results, we evaluated the polarizabilities $\alpha^s_{\text{cont}}(\omega)$ for the clock

levels resulting from transitions to the continuous spectrum [Fig. 3(b)].

The contributions $\alpha_{cont}^s(\omega)$ are small compared to the contribution from the discrete spectrum and differ only by 2 a.u. for the clock levels. This means that the transitions to continuum basically do not influence positions of magic wavelengths. We also assume that the corresponding contribution to the tensor polarizability is even smaller and will neglect it in further analysis. Since the discrete spectrum gives the equal static scalar polarizabilities for the clock levels, we expect the continuous spectrum to contribute to polarizabilities of both levels equally as well. Thus, a rough estimation of the error of differential polarizability caused by the continuous spectrum is about the difference between $\alpha_{cont}^s(0)$ for the clock levels, i.e., 2 a.u. Unfortunately, we do not know of any experimental data on the photoionization cross sections for Tm atoms and therefore can't rigorously estimate the error.

C. Magic wavelength

The magic wavelengths for optical traps, which provide vanishing total light shifts of clock transitions (1), are widely used in optical clocks [9]. To determine the magic wavelengths, one should search for the crossing points of the dynamic polarizabilities for the upper and lower clock levels (neglecting the contribution from the hyperpolarizability in the first approximation). Positions of magic wavelengths strongly depend on energies and probabilities of the resonances in the atom. In general, we can't only use results of our calculations due to insufficient accuracy provided by the COWAN package (see the Appendix).

To solve this problem, first we tried a "combined" approach. Calculated transitions were assigned to experimental ones which can be done unambiguously for wavelengths $\lambda > 500$ nm. It turns out to be impossible for the shorter wavelengths ($\lambda < 500$ nm) due to a higher density of transitions. Then we combined the calculated spectrum for $\lambda < 500$, the available experimental data for $\lambda > 500$ nm, and calculated probabilities for known transitions without measured probabilities. After detailed study we concluded that it is a questionable approach because the calculated and experimentally measured transition probabilities sometimes differ by an order of magnitude see Fig. 9(b). This difference impacts the calculated polarizabilities in a wide spectral range impeding reliable prediction of the magic wavelengths.

In our opinion, a more reliable approach is based on maximal use of calculation results: We took the calculated spectrum and substituted the predicted wavelengths with correct ones known from the experiment for all transitions with $\lambda > 500$ nm. As for the probabilities, we used the calculated ones except for the case when the probability is smaller than 10^5 s^{-1}. This method gives reliable results for the magic wavelengths in the near-IR region with a low density of strong transitions.

The selected approach predicts a reliable candidate for the magic wavelength at 807 nm with an attractive lattice potential (Fig. 4). Its presence is caused by the weak transition from the $|J = 5/2\rangle$ clock level $4f^{13}(^2F^o)6s^2(J = 5/2)$ with the energy 8771.24 to $4f^{12}(^3F_4)5d_{3/2}6s^2(J = 5/2)$ with the energy 21161.4 cm^{-1} at 807.1 nm [37]. At the same time,
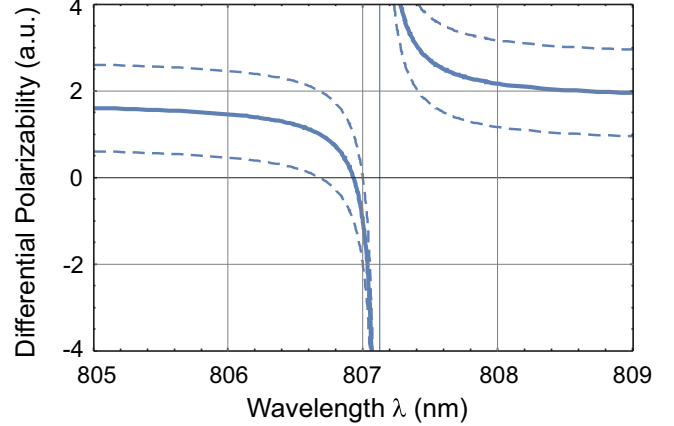

FIG. 4. The magic wavelength for the $1.14\,\mu$m clock transition in the Tm atom ($|m = 0\rangle \rightarrow |m = 0\rangle$) around 807 nm calculated for the linear vertical polarization of the trapping light (see Fig. 2). The solid curve is the differential polarizability of the lower $|J = 7/2, F = 4, m = 0\rangle$ and the upper $|J = 5/2, F = 3, m = 0\rangle$ clock states. The dashed curves show the anticipated uncertainty in the calculation of the differential polarizability which may impact the position of the magic wavelength. The thin vertical line denotes the position of the weak resonance at 807.1 nm discussed in the text.

there are no allowed transitions from the $|J = 7/2\rangle$ clock level in the vicinity of 807 nm. Taking into account the uncertainty in the contribution of the continuous spectra to the evaluated differential polarizability of ± 1 a.u., the proposed magic wavelength should be blue detuned from the transition 807.1 by 0.1 to 1 nm.

The figures-of-merit for an optical lattice come from its depth, the off-resonant scattering rate, and the magnetic dipole-dipole relaxation rate. The optical lattice depth in kelvins is given by

$$U\,[\text{K}] = \alpha[\text{a.u.}]\frac{2\pi a_0^3}{c\,k_B}I\,[\text{W/m}^2], \qquad (8)$$

where I is the field intensity in lattice antinodes given in W/m^2 and k_B is the Boltzmann constant. The spontaneous decay following the off-resonant excitation by the lattice field perturbs the coherence of the clock levels and should be taken into account. The off-resonance scattering rate for the transition $|m = 0\rangle \rightarrow |m = 0\rangle$ can be estimated as [34]

$$\Gamma(\omega)_{0\rightarrow 0} = I \sum_{F'}{}' \frac{\omega_{F'F}^2 + \omega^2}{\left[\omega_{F'F}^2 - \omega^2\right]^2} \frac{3\pi c^2 A_{F'\rightarrow F}}{\hbar\omega_{F'F}^3}$$
$$\times \begin{pmatrix} F_u & 1 & F_d \\ 0 & 0 & 0 \end{pmatrix}^2 (2F_u + 1)\Gamma_{F_u}, \qquad (9)$$

where Γ_{F_u} is the inverse lifetime of $|F_u\rangle$ level.

The optical lattice at 807 nm can be formed by a Ti:sapphire laser beam. With 0.5 W output power focused in the beam waist of 50 μm (radius at $1/e^2$ intensity level) corresponding to $I = 50$ kW/cm^2 in the retroreflected configuration, one expects the trap depth of 20 μK. This is enough to capture Tm atoms from a narrow-line magneto-optical trap (MOT). Even for the smallest expected detuning from the 807.1 resonance of 0.1 nm, the off-resonant scattering rate is less than 0.1 s^{-1}.

D. Hyperpolarizability

The magic wavelength depends not only on the differential polarizability of the clock states, but also on the differential hyperpolarizability (1) and light intensity I. The scalar hyperpolarizability $\gamma(\omega)$ is given by [43]

$$\gamma(\omega) = \tfrac{1}{4}[\gamma^+(\omega) + \gamma^-(\omega)], \tag{10}$$

where

$$\gamma^+ = \frac{4}{\hbar^3} {\sum}'_{m,k,n} (D_z)_{gm}(D_z)_{mk}(D_z)_{kn}(D_z)_{ng}$$

$$\times \left(\frac{4\omega_{mg}\omega_{ng}}{\omega_{kg}(\omega^2 - \omega_{mg}^2)(\omega^2 - \omega_{ng}^2)} \right.$$

$$+ \frac{1}{(\omega_{mg} - \omega)(\omega_{kg} - 2\omega)(\omega_{ng} - \omega)}$$

$$\left. + \frac{1}{(\omega_{mg} + \omega)(\omega_{kg} + 2\omega)(\omega_{ng} + \omega)} \right) \tag{11}$$

and

$$\gamma^- = \frac{8}{\hbar^3} {\sum}'_{m,n} |(D_z)_{mg}|^2 |(D_z)_{ng}|^2$$

$$\times \frac{\omega_{mg}(\omega^2 + 3\omega_{ng}^2)}{(\omega^2 - \omega_{mg}^2)(\omega^2 - \omega_{ng}^2)^2}, \tag{12}$$

where $(D_z)_{i,j}$ is a matrix element of the z projection of the dipole moment between levels i and j.

To calculate the hyperpolarizability we used the transition matrix elements, their signs, and the transition wavelengths obtained by the COWAN package for all transitions except the 807.1 nm one. For this transition, we used the experimentally measured wavelength and probability; the sign of the transition matrix element was taken from the numerical calculations. This exception is done to improve accuracy of the magic wavelength prediction.

The light shifts for the clock levels $|J = 7/2\rangle$ and $|J = 5/2\rangle$ coming from the hyperpolarizabilities in the optical lattice at $\lambda = 807$ nm and $I = 50\,\text{kW/cm}^2$ is shown in Fig. 5. As shown in the previous section, the magic wavelength is blue detuned from the 807.1 nm resonance by more than 0.1 nm, which makes the hyperpolarizability shift to be less than 0.5 Hz. The corresponding correction to the magic wavelength is negligible. Still, hyperpolarizability contributes to the clock frequency uncertainty which is discussed later in Sec. IV.

III. MAGNETIC INTERACTIONS

A. Magnetic dipole-dipole interaction

The magnetic moment of the thulium ground state equals $4\mu_B$ (μ_B is the Bohr magneton) which causes a magnetic dipole-dipole interaction between atoms. The interaction potential between two atoms is

$$\hat{U}_{dd}(r) = \mu_0(g_F\mu_B)^2 \frac{\hat{\vec{F}}_1 \cdot \hat{\vec{F}}_2 - 3(\hat{\vec{F}}_1 \cdot \hat{r})(\hat{\vec{F}}_2 \cdot \hat{r})}{4\pi r^3}, \tag{13}$$

where $\vec{F}_{1,2}$ are the total atomic angular momenta, μ_0 is the magnetic permeability of vacuum, $\vec{r}$ is the vector pointing
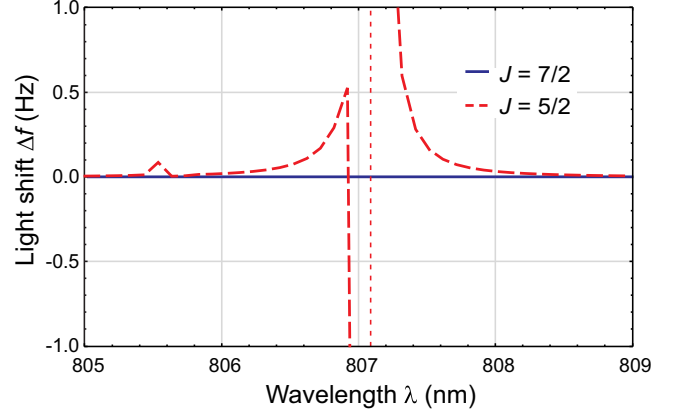

FIG. 5. Light shifts of the lower $|J = 7/2\rangle$ (blue, solid) and upper $|J = 5/2\rangle$ (red, dashed) clock levels caused by the hyperpolarizability. Vertical red line denotes the position of the resonance. Calculations are done for an intensity of $I = 50\,\text{kW/cm}^2$; the hyperfine interaction is ignored.

from one atom to another, and g_F is the Landé g factor of the ground state. For the Tm ground state $g_F \approx 1$.

For spatially nonuniform atom distributions over optical lattice sites, the magnetic interaction may lead to inhomogeneous broadening and frequency shifts of the clock transition, both of them being of the same order of magnitude. These shifts correspond to the interaction energy between neighboring atoms. For two Tm atoms loaded in the adjacent sites of the optical lattice at 800 nm and prepared in the $|m = 4\rangle$ magnetic state, the interaction energy (13) corresponds to the frequency shift of

$$\Delta f_{dd} \approx \frac{\mu_0(m\,\mu_B)^2}{4\pi r^3 h}, \tag{14}$$

which is of the order of 10 Hz. The shift is large and difficult to predict due to the randomness of the lattice site occupation. For the rest of the paper, we will analyze only the transition $|m = 0\rangle \rightarrow |m = 0\rangle$ which is insensitive to this shift.

Magnetic dipole-dipole interactions also limit the interrogation time because of spin relaxation: the atomic ensemble prepared into a pure polarized state will gradually lose its polarization. To evaluate the corresponding relaxation time, we solved the Schrödinger equation with the interaction (13) for two, three, four, and five spatially fixed Tm atoms in the ground state ($F_1 = F_2 = 4$) prepared in the initial $|m = 0\rangle \otimes \cdots \otimes |m = 0\rangle$ state at the vanishing external magnetic field. The spatial separation of $a = 400$ corresponds to an 800-nm optical lattice. The relative positions of the atoms are shown in Fig. 6(a). Figure 6(b) shows dynamics of the spin state for the central atom, marked blue in Fig. 6(a).

For two, three, and four atoms the Schrödinger equation was solved exactly. For five atoms the Hilbert space is too large, and we restricted our calculation to the subspace $m_i = \{-2, -1, 0, 1, 2\}$. To estimate validity of this approach we also solved the Schrödinger equation for two, three, and four atoms in the restricted subspace. The inset in Fig. 6(b) shows good agreement between approximate and exact solutions for the first 50 ms of the evolution. In the steady-state, it is reasonable to assume that all spin projections are equiprobable.
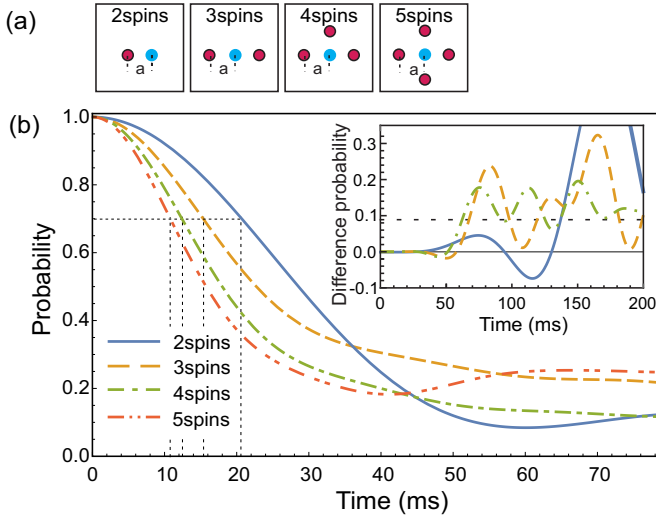
FIG. 6. Spin relaxation dynamics. (a) Configurations of atoms used in the simulation; $a = 400$ nm is the interatomic separation, and quantization axes are perpendicular to the plane of the sketch. (b) Probability to find the central atom (blue) in the state $|m = 0\rangle$ for two, three, four, and five atoms in the 2D-optical lattice. Note, that the probabilities do not go to zero at longer times because at a steady state there is almost uniform distribution among magnetic sublevels. Inset: Difference of the probabilities to find the first atom in the state $|m = 0\rangle$ for exact and approximate solutions for two, three, and four atoms. The horizontal dashed line represents the difference of the steady-state probabilities (see the main text).

Consequently, average probability to find the central spin in the $|m = 0\rangle$ state equals 1/9 for the full Hilbert space and 1/5 for the truncated space. This explains the discrepancy between the exact and approximate solutions at longer times (>50 ms). The characteristic relaxation time was derived by setting the probability to find the central spin in the initial $|m = 0\rangle$ state to 0.7. It equals 20, 13, 11, and 10 ms for two, three, four, and five spins, respectively [Fig. 6(b)].

External magnetic fields reduce spin relaxation because some spinflip processes require additional energy. A significant reduction of the spin relaxation is expected if the Zeeman splitting becomes larger than the kinetic energy E_K of atoms. At the experimentally achieved temperature of $T \sim 10\,\mu$K, the kinetic energy equals $E_K = k_B T \sim 100\,$kHz $\times\,h$. This energy corresponds to a magnetic field of $B \approx E_K/(h\mu_B)$ or approximately 100 mG. We show in the next section that such a bias magnetic field will cause a significant Zeeman shift and cannot not be applied during the clock operation. As mentioned in the Introduction, the temperature can be lowered to a few microkelvins which will reduce the threshold magnetic field to a few tens of milligausses which is sufficient for the clock's target accuracy.

Assuming that the lattice filling factor is less than unity and taking into account the influence of a weak magnetic bias field (10 mG), we conclude that the spin relaxation time should be larger than 10 ms. This sets the bound for the interrogation time of the clock transition and, correspondingly, its Fourier-limited spectral linewidth of < 10 Hz. As a result, the spin relaxation should not considerably impact the performance of the proposed optical clock.

B. Interaction with an external magnetic field

To selectively address the $|m = 0\rangle \to |m = 0\rangle$ transition, an external static magnetic field B_0 has to be applied. The Hamiltonian describing hyperfine interaction for the ^{169}Tm atom ($I = 1/2$) in the presence of the external magnetic field B_0 is [44]:

$$\hat{H} = hA\hat{\vec{I}} \cdot \hat{\vec{J}} - g_I \mu_N \hat{\vec{I}} \cdot \hat{\vec{B}}_0 - g_J \mu_B \hat{\vec{J}} \cdot \hat{\vec{B}}_0, \quad (15)$$

where A is the hyperfine constant, g_I is the nuclear Landé g factor, μ_N is the nuclear magneton, and g_J is the electronic Landé g factor. The well-known Breit-Rabi formula gives eigenvalues for the special case of $J = 1/2$. Making the formal substitution $I \leftrightarrow J$, $g_I \leftrightarrow g_J$, $\mu_N \leftrightarrow \mu_B$ in (15), one can use the Breit-Rabi expression for $I = 1/2$ [44]. The frequency shift of the clock transition $|m = 0\rangle \to |m = 0\rangle$ is given by

$$\Delta f_{0\to 0} = \frac{(g_{5/2}\mu_B - g_I \mu_N)^2 B_0^2}{4h^2 \Delta W_{5/2}}$$
$$- \frac{(g_{7/2}\mu_B - g_I \mu_N)^2 B_0^2}{4h^2 \Delta W_{7/2}} = \beta B_0^2 \quad (16)$$

and

$$\beta = -257(1)\,\text{Hz/G}^2, \quad (17)$$

where $\Delta W_{7/2} = 1496.550(1)$ and $\Delta W_{5/2} = 2114.946(1)$ MHz are the hyperfine frequency splittings of the $|J = 7/2\rangle$ and $|J = 5/2\rangle$ clock levels, respectively [45], $g_{7/2} = 1.141189(3)$ [44] and $g_{5/2} = 0.855(1)$ [46] are their Landé g factors, and $g_I = 0.462(3)$ is the nuclei Landé g factor [44].

IV. Tm CLOCK UNCERTAINTY

Here we will discuss the most significant sources of uncertainty for the proposed Tm clock.

A. Black body radiation

The frequency shift of the clock transition due to the ac-Stark shift induced by BBR is given by

$$\Delta f_{BBR} = \int_{\omega=0}^{\infty} \frac{a_0^3 \omega^3}{\pi^2 c^2} \frac{[\alpha_{gr}^s(\omega) - \alpha_{cl}^s(\omega)]}{e^{\frac{\hbar\omega}{k_B T}} - 1} d\omega$$
$$\approx \Delta\alpha_0^s \frac{a_0^3 \pi^2 k_B^4}{15 c^3 \hbar^4} T^4 = 1.17 \times 10^{-12}\,\Delta\alpha_0^s\,[\text{a.u.}]\,T^4\,[\text{K}],$$
$$(18)$$

where $\Delta\alpha_0^s$ is the differential scalar static polarizability of the clock levels in atomic units, and T is the temperature in kelvin.

Our calculations (see Sec. II) give $\Delta\alpha_0^s = 2$ a.u. which results in $\Delta f_{BBR} = 20$ mHz at $T = 300$ K. It corresponds to a fractional frequency shift of the clock transition of 8×10^{-17} which is much less than for the Sr atom and is comparable to Al$^+$ clock transition [35]. Uncertainty of the ambient temperature of 3 K will introduce a frequency uncertainty of 3×10^{-18} (0.8 mHz). Since there are no strong transitions from the clock levels in the infrared region, the dynamic BBR shift is negligibly small [47].

B. Second order Zeeman shift

According to (16), the frequency shift of the clock transition in the external magnetic field of $B_0 = 10$ mG corresponds to $-25.7(1)$ mHz or 10^{-16} in fractional units. One can accurately measure the bias field B_0 by monitoring the Zeeman shift of the $|m = -4\rangle \to |m = -3\rangle$ and $|m = 4\rangle \to |m = 3\rangle$ transitions [48]. The frequency splitting of these magnetic sensitive transitions in a magnetic field is equal to $\xi = 2(4g_{J=7/2,F=4} - 3g_{J=5/2,F=3})\mu_B/h = 6.00(2)$ MHz/G, where $g_{J=7/2,F=4}$ and $g_{J=5/2,F=3}$ are the Landé g factors of the states $|J = 7/2, F = 4\rangle$ and $|J = 5/2, F = 3\rangle$, respectively. Given that the linewidths of both transitions are smaller than $\delta f_{4\to3} = 100$ Hz [the broadening due to the magnetic interaction (18) is included], the bias magnetic field B_0 can be measured *in situ* with the uncertainty of $\Delta_{B_0} = \delta f_{4\to3}/\xi \leqslant 0.1$ mG. Since the magnetic field can be stabilized at the same level over the interrogation sequence [49], we take 0.1 mG as an upper limit for the bias magnetic field instability and estimate the quadratic Zeeman shift's contribution as $2\beta B_0 \Delta B_0 = 0.5$ mHz (2×10^{-18} in fractional units) after correction.

C. Dynamic light shifts

Fluctuations δI of the laser intensity cause shifts and broadening of the clock transition originated from the nonzero differential hyperpolarizability $\Delta\gamma$:

$$\Delta f_I = -\frac{\delta I}{I}\left(\frac{\Delta\alpha}{4}I + 2\frac{\Delta\gamma}{64}I^2\right) = -\frac{\delta I}{I}\frac{\Delta\gamma}{64}I^2, \quad (19)$$

where we take into account that

$$\frac{\Delta\alpha}{4}I + \frac{\Delta\gamma}{64}I^2 = 0 \quad (20)$$

at the magic wavelength. Previously, we estimated that $\Delta\gamma/64 \times I^2$ is less than 0.5 Hz for the given lattice parameters (see Sec. II D). Stabilizing the laser intensity at the level of 10^{-3} can reduce the uncertainty in the frequency of the clock transition to 0.5 mHz or 2×10^{-18} in fractional units.

D. van der Waals and quadrupole interactions

The electrostatic van der Waals interaction between two neutral atoms shifts the clock frequency by $-(C_6 a_B^6 E_H)/(h\,r^6)$, where C_6 is the van der Waals coefficient in atomic units, a_B is the Bohr radius, and E_H is the Hartree energy. Following [50], we estimated $C_6 \sim 6000$ a.u. for the $|J = 7/2\rangle$ level. For an atomic separation of $r = 400$ nm (atoms are placed in the 800-nm optical lattice, less than one atom per site) the van der Waals frequency shift is less than 0.1 mHz which corresponds to 4×10^{-19} in fractional units.

To estimate the contribution from the quadrupole-quadrupole interaction, we calculated the quadruple moment for the ground state of the Tm atom using the COWAN package. The result is $D \sim 0.5\,ea_B^2$ (e is the elementary charge). The corresponding frequency shift is $D^2/(4\pi\epsilon_0 r^5 h) < 0.1$ mHz.

E. Line pulling and geometrical effects

In an external bias magnetic field of $B_0 = 10$ mG, the $|J = 7/2, F = 4\rangle \to |J = 5/2, F = 3\rangle$ transition will be split into magnetic components. The line pulling effect [51] can perturb the magnetic-insensitive clock $|m = 0\rangle \to |m = 0\rangle$ transition. Imperfect coalignment of the magnetic field B_0 and the polarization of the interrogating laser beam (Fig. 2) leads to excitation of $|m = 0\rangle \to |m = \pm1\rangle$ transitions and also can cause the line pulling effect.

In both cases, the separation from the clock transition to the nearest transition is not less than $10^3\gamma \approx 20$ kHz, where $\gamma = 20$ Hz is the upper bound for the expected transition linewidth. The corresponding incoherent line pulling is negligible ($< 10^{-8}$ Hz) and does not impact the clock performance. For reading the clock transition, absorption spectroscopy is typically used and we do not expect a contribution from the coherent line pulling [52].

Another systematic effect related to the geometry can come from misalignment of the lattice light polarization and the bias magnetic field (see Fig. 2). The shift results from the differential tensor polarizability of the clock levels $\Delta\alpha^t$ and scales as the square of the misalignment angle [53]. It was shown that the corresponding relative frequency shift can be reduced to less than 2×10^{-18} by proper alignment [53].

F. Uncertainty budget

The list of dominant frequency shifts and corresponding uncertainties is presented in Table I. The major line shifts are the BBR shift and the second-order Zeeman shift. All of these can be well characterized and corrected to a high degree using moderate assumptions and established experimental techniques. Light shift can also be controlled at a low 10^{-18} level by intensity stabilization of the light field. As a result, the systematic frequency uncertainty of the proposed Tm optical clock at 1.14 μm can be reduced to 5×10^{-18} in fractional units.

For the 10 Hz clock transition (see Sec. III A), an interrogation duty cycle of 1%, and an ensemble of 10^5 trapped Tm atoms, we expect the Allan deviation of $10^{-15}/\sqrt{\tau}$ (here τ is the averaging time) [54]. It is only 3 times inferior to the ^{87}Sr optical clock [12]. To reach the estimated fractional uncertainty of 5×10^{-18} in Tm, the integration time should be less than 5×10^4 s.

V. EXPERIMENT

The experimental section describes our measurement of the $|J = 5/2\rangle$ clock level lifetime in a dilute cloud of cold Tm atoms. Formerly, the decay from this level was studied in Tm atoms implanted in solid and liquid ^{4}He [55]. Strong shielding of inner shells and the high symmetry of the perturbing field of the He matrix give the impressive result of 75(3) ms for the lifetime of the $|J = 5/2\rangle$ clock level. Note that the level was populated by a cascade decay from highly excited levels.

In contrast to [55], we directly excite the $|J = 7/2, F = 4\rangle \to |J = 5/2, F = 3\rangle$ transition by spectrally narrow laser radiation at 1.14 μm in an ensemble of Tm atoms trapped in a 1D-optical lattice and measure the lifetime of the $|J = 5/2\rangle$ clock level monitoring its decay to the ground $|J = 7/2,$

TABLE I. Uncertainty budget for a Tm optical clock operating at the $1.14\,\mu$m magnetic dipole transition. Atoms are trapped in the 2D-optical lattice at the magic wavelength close to 807 nm with the light intensity of 50 kW/cm^2.

Contribution	Frequency shift (mHz)	Uncertainty after correction (mHz)	Uncertainty in fractional units (10^{-18})
BBR ($T = 300 \pm 3$ K)	20	0.8	3
Zeeman shift ($B_0 = 10.0 \pm 0.1$ mG)	-26	0.5	2
Light shift due to hyperpolarizability($\delta I/I = 10^{-3}$)	0	0.5	2
Light shift due to tensor polarizability	0.5	0.5	2
van der Waals and quadrupole interaction	0.1	0.1	0.4
Total	-6	1.2	< 5

$F = 4\rangle$ state. Besides that, we evaluated dynamic polarizability of Tm atoms at 532 nm by exciting parametric resonances in an optical lattice.

A. Lifetime of the $|J = 5/2\rangle$ clock level

The lifetime of the $|J = 5/2\rangle$ clock level is measured by excitation of the magnetic dipole transition at 1.14 μm in a 1D-optical lattice. About 10^6 thulium atoms are laser cooled down to 20 μK in a narrow-line MOT operating at 530.7 nm [22] and then are recaptured by the 1D-optical lattice. The lattice is formed by a retroreflected focused 532 nm cw laser beam (waist radius is 50 μm, laser power is 3 W) and superimposed with the atomic cloud. The trap depth is calculated to be 400 μK for the ground $|J = 7/2, F = 4\rangle$ state which provides a recapture efficiency of 40% [22].

After recapture (pulse 1 in Fig. 7), we switch the MOT off and wait for 20 ms to let uncaptured atoms escape. Then, a resonant 1.14 μm laser pulse of 30 ms (pulse 2) is applied to excite atoms to the $|J = 5/2, F = 3\rangle$ level [30]. The laser is actively stabilized to a high-finesse ultra-low expansion cavity [23] which narrows the laser spectral linewidth down to ~ 10 Hz. After the interrogation pulse, a resonant 410.6 nm laser pulse of 1 ms (pulse 3) is applied to remove atoms from the $|J = 7/2\rangle$ ground state (Fig. 1). Atoms exited to the $|J = 5/2, F = 3\rangle$ decay back to the $|J = 7/2, F = 4\rangle$ ground state, whose population is monitored by a fluorescence signal induced by a delayed 410.6 nm probe pulse (pulse 4).

The increase of the population of the $|J = 7/2, F = 4\rangle$ ground state is described by the exponential function

$$N(t) = N_0[1 - \exp(-t/\tau)], \qquad (21)$$

where τ is the lifetime of the the excited $|J = 5/2, F = 3\rangle$ state and N_0 is the initial number of atoms in this state. By fitting the experimental data presented in Fig. 7, we measure $\tau = 112(4)$ ms. It is the lower bound for the $|J = 5/2\rangle$ level natural lifetime since the measured lifetime can be reduced by additional weak losses from the $|J = 5/2\rangle$ level in the optical lattice. These losses may be related to optical or magnetic Feshbach resonances [56].

Thus, the natural linewidth of the clock transition $|J = 7/2\rangle \rightarrow |J = 5/2\rangle$ is expected to be not broader than 1.4 Hz which is consistent with the previous measurement in ^{4}He matrix [55] and the theoretical prediction of 1.14 Hz [57]. The natural linewidth of the transition does not limit the performance of the proposed optical clock (see Sec. IV), because for most routinely operating optical clocks the Fourier-limited spectral linewidth of the clock transition is on the order of 10 Hz.

In the current experimental arrangement we observed the spectral linewidth of the $|J = 7/2, F = 4\rangle \rightarrow |J = 5/2, F = 3\rangle$ transition of 1 MHz at the low power limit [25]. The line was broadened by the Zeeman effect in the uncompensated laboratory field (~ 0.5 MHz) and by an inhomogeneous ac-Stark shift caused by a large differential dynamic polarizability of the clock levels at 532 nm (~ 0.4 MHz).
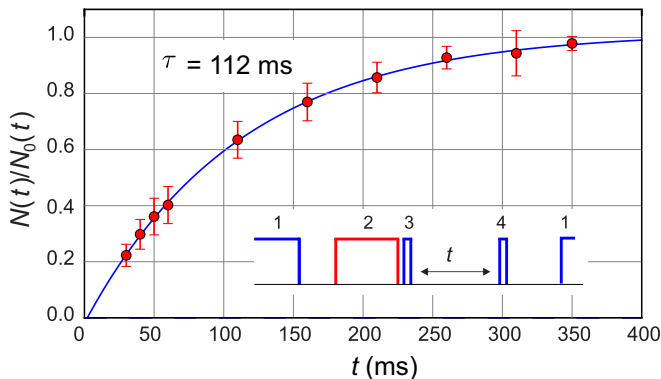

FIG. 7. Measurement of the lifetime of the $|J = 5/2\rangle$ level. Red dots are the normalized number of atoms decayed to the ground $|J = 7/2, F = 4\rangle$ level. The solid curve is a fit by (21). The inset shows the pulse sequence described in the text.

B. Parametric resonances

The dynamic polarizability of the $|J = 7/2\rangle$ ground state at the lattice wavelength can be evaluated by the excitation of parametric resonances in the lattice and by monitoring the corresponding losses [58]. This method is very sensitive to the laser beam parameters (waist size, astigmatism) and does not allow accurate comparison to our calculations. Still, it gives the proper order of magnitude for the polarizability and provides unambiguous proof that Tm atoms are localized in the 1D-optical lattice.

At low temperatures, atomic motion in the optical lattice becomes quantized and the corresponding axial f_a and radial f_r oscillation frequencies at the center of the lattice are
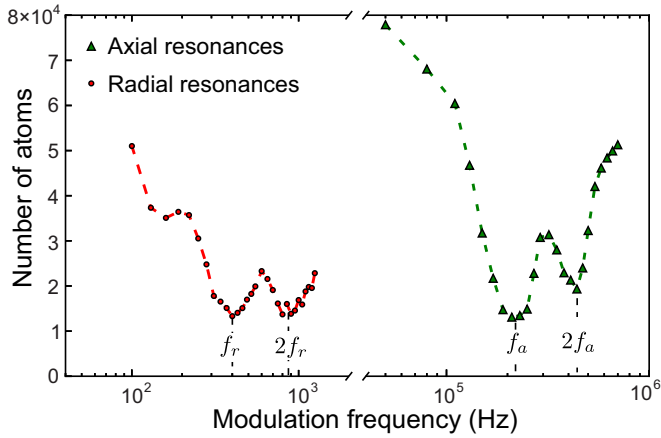
FIG. 8. Excitation of the parametric resonances in the 532 nm 1D-optical lattice. Green triangles are axial resonances; red circles are radial ones; and dashed curves are guides to the eyes.

given by

$$f_a = \frac{4}{w_0 \lambda} \sqrt{\frac{2 a_0^3 \alpha^s P}{c m_0}},$$

$$f_r = \frac{4}{\pi w_0^2} \sqrt{\frac{a_0^3 \alpha^s P}{c m_0}},$$
(22)

where $P = 4$ W is the optical power of the laser beam forming the 1D lattice, m_0 is the Tm atomic mass, w_0 is the beam waist radius (at $1/e^2$ intensity level), $\lambda = 532$ nm is the lattice wavelength, and α^s is the scalar polarizability at $\lambda = 532$ nm of the $|J = 7/2, F = 4\rangle$ level in atomic units. According to [59], harmonic modulation of the trap depth at frequencies $2f/n$ [here f is one of the eigenfrequencies (22) and n is an integer] will cause parametric excitation of the resonances and corresponding trap losses.

To excite parametric resonances in the 532 nm optical lattice, we harmonically modulated the laser power and, correspondingly, the trap depth by an acousto-optical modulator (AOM) at the level of 10%. The number of atoms remaining in the optical lattice after 100 ms of parametric excitation was monitored by resonance fluorescence at 410.6 nm. The corresponding spectrum is shown in Fig. 8. The low frequency parametric resonances at 400(40) and 900(150) Hz correspond to the radial oscillations at f_r and $2f_r$ frequencies. The high frequency resonances at 230(40) and 420(50) kHz are related to axial oscillations at f_a and $2f_a$ in the tight potential wells of the lattice. Higher order parametric resonances are much weaker and broader [59] and were not observed.

The scalar polarizability can be deduced from (22) by excluding w_0:

$$\alpha^s = \frac{f_a^4 \lambda^4 c m_0}{64 f_r^2 a_0^3 \pi^2 P}.$$
(23)

From the measured frequencies we estimate this value to be 360^{+300}_{-200} which agrees with the calculated polarizability of 600 a.u. within error bars. The main sources of uncertainty are astigmatism in the lattice beams, axial and radial misalignment of the waist positions of the lattice beams, and error in our determination of the parametric resonance frequency.

In conclusion, the experimental results for the scalar dynamic polarizability α^s at 532 nm in the optical lattice and in the dipole trap are consistent with the calculated value of 600 a.u. Although the experiment does not allow us to test the accuracy of our calculations, it unambiguously proves trapping Tm atoms in the optical lattice at 532 nm.

VI. SUMMARY

We considered the possibility to use the inner-shell transition $[Xe]4f^{13}6s^2(J = 7/2, F = 4, m = 0) \rightarrow [Xe]4f^{13}6s^2(J = 5/2, F = 3, m = 0)$ in the Tm atom at $\lambda = 1.14\,\mu$m as a candidate for an optical lattice clock. The transition wavelengths and probabilities for two clock levels $|J = 7/2\rangle$ and $|J = 5/2\rangle$ in the spectral range 250–1200 nm are calculated using the COWAN package. We calculate the differential dynamic polarizability and predict the magic wavelength at 807 nm with an attractive optical potential. Our results show a reasonable correspondence with existing experimental data and significantly extend it to the UV and IR spectral ranges.

The suggested clock transition demonstrates a low sensitivity to the BBR shift which provides a clock frequency accuracy at the low 10^{-18} level competing with the best known optical clocks. We also evaluated other feasible contributions to clock performance (magnetic interactions, light shifts, van der Waals, and quadrupole shifts) which, after reasonable assumptions, can be lowered to the 10^{-18} level. Together with the relative simplicity of laser cooling and trapping of Tm atoms, our results demonstrate that Tm is a promising candidate for optical clock applications. One of the disadvantages is the relatively low carrier frequency of only 2.6×10^{14} Hz which requires longer integration time to reach the same instability as Sr and Yb lattice clocks.

Our experiments with direct excitation of the clock transition by spectrally narrow laser radiation at $\lambda = 1.14\,\mu$m set a lower limit for the upper clock level lifetime of 112 ms which corresponds to the natural linewidth of < 1.4 Hz. Experiments are done in a 1D-optical lattice at 532 nm. Modulating the trap depth and analyzing the corresponding parametric resonances frequencies, we deduce the scalar polarizability of the Tm ground state at 532 nm which shows reasonable agreement with our calculations.

To experimentally study the magic wavelength and analyze systematic shifts, we plan to change the trapping wavelength to 806 to 807 nm using a tunable Ti:sapphire laser. This will also simplify our study of Feshbach resonances and may open a way to study and control dipole-dipole interactions using narrow band excitation of the clock transition at 1.14 μm.
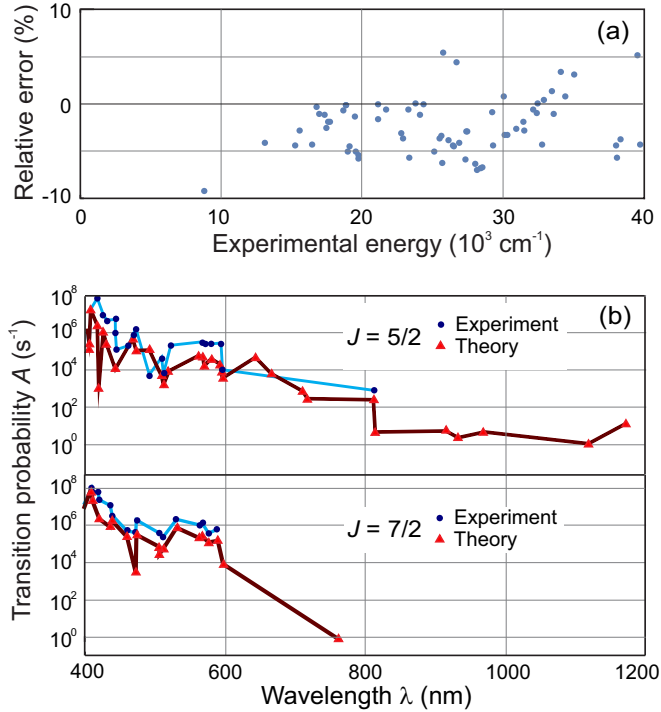
FIG. 9. Comparison between the calculated and measured data. Only levels which were identified with the experimentally measured ones are shown. (a) Relative error of calculated energy levels. (b) Calculated (red triangles) and measured (blue circles) transition probabilities from the upper $|J = 5/2\rangle$ and the lower $|J = 7/2\rangle$ clock levels. Solid curves are guides for the eyes only.

APPENDIX: TRANSITION PROBABILITIES

Calculation of dynamic polarizabilities Eqs. (3)–(5) requires knowledge of electrical dipole transition rates from the lower $|J = 7/2\rangle$ and the upper $|J = 5/2\rangle$ clock levels in Tm. A number of transitions rates were experimentally measured and the results are summarized in [37]. We completed this list calculating energy levels in the range up to 40 000 cm^{-1} and corresponding transition-dipole matrix elements using the COWAN package [39] taking into account the low lying odd $(4f^{13}6s^2, 4f^{13}5d^16s^1, 4f^{12}6s^26p^1, 4f^{13}6p^2,$ and $4f^{13}5d^2)$ and even $(4f^{12}5d^16s^2$ and $4f^{13}6s^16p^1)$ configurations.

As follows from Fig. 9(a), the accuracy of the calculated level energies is better than 20%. Together with the known leading configuration percentage it is sufficient to identify the low lying levels with the energies $E < 20\,000$ cm^{-1} ($\lambda > 500$ nm) and compare them with the experimentally measured ones [60]. Table II shows calculated probabilities of the transitions with experimentally unknown probabilities from

TABLE II. Calculated transition probabilities (experimentally unknown) from the $|J = 7/2\rangle$ and $|J = 5/2\rangle$ clock levels. E and J are experimentally measured energies and electronic angular momenta of the upper levels of the transitions, respectively.

E (10^3 cm^{-1})	J	λ (nm)	A (s^{-1})
	$\|J = 7/2\rangle$ level		
13 119.6	9/2	762.22	3.2
16 742.2	7/2	597.29	1.9×10^5
19 748.5	9/2	506.37	1.2×10^6
	$\|J = 5/2\rangle$ level		
16 742.2	7/2	1254.55	14.1
16 957.0	7/2	1221.63	1.2
17 343.4	7/2	1166.57	171.2
17 752.6	5/2	1113.41	27.5
19 132.2	3/2	965.16	150
19 548.8	5/2	927.85	100
19 753.8	7/2	910.53	209
21 120.8	7/2	809.74	640
22 791.2	7/2	713.27	27 400
22 929.7	5/2	706.29	58 900
23 873.2	7/2	662.17	1×10^6
23 882.4	3/2	661.76	2.13×10^6
24 418.4	5/2	639.11	1.79×10^7

the clock levels [Xe]$4f^{13}6s^2$ ($J = 7/2$) and [Xe]$4f^{13}6s^2$ ($J = 5/2$). Figure 9(b) compares experimentally measured and calculated probabilities for identified transitions in the range 400–1200 nm. Taking into account difficulties with the simulation of the hollow-shell atomic potentials [34], the discrepancy between the calculated and the experimental data seems to be reasonable.

As mentioned in the main text, the most self-consistent approach for deriving differential polarizability of the clock levels is to use the calculated data for the transition probabilities; otherwise we meet difficulties with level identification in the wavelength range $\lambda < 500$ nm and with matching the calculated and the experimental data. In turn, transitions to the highly excited Rydberg states ($\lambda < 250$ nm) become extremely dense and the COWAN package cannot be used. To calculate their contribution, one typically uses a semianalytical approach [61]. In our case, the strong similarity of spectra starting from two inner-shell fine structure sublevels—clock levels ($|J = 7/2\rangle$ and $|J = 5/2\rangle$)—results in a very small differential polarizability of 0.1 a.u. if one takes into account all transitions in the spectral range 250–1200 nm. Transitions to the Rydberg states may slightly influence the absolute values of the polarizability of the clock states (at the level of a few a.u.), but we do not expect a significant contribution to the differential polarizability $\Delta\alpha$.

[1] E. V. Zharikov, V. I. Zhekov, L. A. Kulevskii, T. M. Murina, V. V. Osiko, A. M. Prokhorov, A. D. Savel'ev, V. V. Smirnov, B. P. Starikov, and M. I. Timoshechkin, Sov. J. Quantum Electron. **4**, 1039 (1975).

[2] N. P. Barnes, E. D. Filer, F. L. Naranjo, W. J. Rodriguez, and M. R. Kokta, Opt. Lett. **18**, 708 (1993).

[3] T. Böttger, G. J. Pryde, N. M. Strickland, P. B. Sellin, and R. L. Cone, Opt. Photonics News **12**, 23 (2001).

[4] G. Wilpers, T. Binnewies, C. Degenhardt, U. Sterr, J. Helmcke, and F. Riehle, Phys. Rev. Lett. **89**, 230801 (2002).

[5] T. Ido, T. H. Loftus, M. M. Boyd, A. D. Ludlow, K. W. Holman, and J. Ye, Phys. Rev. Lett. **94**, 153001 (2005).

[6] E. B. Aleksandrov, V. D. Vedenin, and V. N. Kulyasov, Opt. Spectrosc. **56**, 365 (1984).

[7] C. I. Hancox, S. C. Doret, M. T. Hummon, L. Luo, and J. M. Doyle, Nature (London) **431**, 281 (2004).

[8] C. B. Connolly, Y. S. Au, S. C. Doret, W. Ketterle, and J. M. Doyle, Phys. Rev. A **81**, 010702 (2010).

[9] H. Katori, M. Takamoto, V. G. Pal'chikov, and V. D. Ovsiannikov, Phys. Rev. Lett. **91**, 173005 (2003).

[10] M. Takamoto and H. Katori, Phys. Rev. Lett. **91**, 223001 (2003).

[11] A. D. Ludlow, M. M. Boyd, J. Ye, E. Peik, and P. O. Schmidt, Rev. Mod. Phys. **87**, 637 (2015).

[12] B. J. Bloom, T. L. Nicholson, J. R. Williams, S. L. Campbell, M. Bishof, X. Zhang, W. Zhang, S. L. Bromley, and J. Ye, Nature (London) **506**, 71 (2014).

[13] N. Hinkley, J. A. Sherman, N. B. Phillips, M. Schioppo, N. D. Lemke, K. Beloy, M. Pizzocaro, C. W. Oates, and A. D. Ludlow, Science **341**, 1215 (2013).

[14] K. Beloy, N. Hinkley, N. B. Phillips, J. A. Sherman, M. Schioppo, J. Lehman, A. Feldman, L. M. Hanssen, C. W. Oates, and A. D. Ludlow, Phys. Rev. Lett. **113**, 260801 (2014).

[15] M. S. Safronova, S. G. Porsev, U. I. Safronova, M. G. Kozlov, and C. W. Clark, Phys. Rev. A **87**, 012509 (2013).

[16] I. Ushijima, M. Takamoto, M. Das, T. Ohkubo, and H. Katori, Nat. Photonics **9**, 185 (2015).

[17] A. P. Kulosa, D. Fim, K. H. Zipfel, S. Rühmann, S. Sauer, N. Jha, K. Gibble, W. Ertmer, E. M. Rasel, M. S. Safronova, U. I. Safronova, and S. G. Porsev, Phys. Rev. Lett. **115**, 240801 (2015).

[18] J. J. McFerran, L. Yi, S. Mejri, W. Zhang, S. Di Manno, M. Abgrall, J. Guéna, Y. Le Coq, and S. Bize, Phys. Rev. A **89**, 043432 (2014).

[19] K. Aikawa, A. Frisch, M. Mark, S. Baier, A. Rietzler, R. Grimm, and F. Ferlaino, Phys. Rev. Lett. **108**, 210401 (2012).

[20] M. Lu, N. Q. Burdick, S. H. Youn, and B. L. Lev, Phys. Rev. Lett. **107**, 190401 (2011).

[21] D. Sukachev, A. Sokolov, K. Chebakov, A. Akimov, S. Kanorsky, N. Kolachevsky, and V. Sorokin, Phys. Rev. A **82**, 011405 (2010).

[22] D. D. Sukachev, E. S. Kalganova, A. V. Sokolov, S. A. Fedorov, G. A. Vishnyakova, A. V. Akimov, N. N. Kolachevsky, and V. N. Sorokin, Quantum Electron. **44**, 515 (2014).

[23] J. Alnis, A. Matveev, N. Kolachevsky, T. Udem, and T. W. Hänsch, Phys. Rev. A **77**, 053809 (2008).

[24] T. Kessler, C. Hagemann, C. Grebing, T. Legero, U. Sterr, F. Riehle, M. J. Martin, L. Chen, and J. Ye, Nat. Photonics **6**, 687 (2012).

[25] E. K. Vishnyakova, G. A. Golovizin, A. A. Kalganova, V. N. Sorokin, N. N. Sukachev, D. D. Tregubov, D. O. Khabarova, and K. Yu. Kolachevsky, Phys. Usp. **59**, 168 (2016).

[26] A. Frisch, Dipolar quantum gases of Erbium, Ph.D. thesis, University of Innsbruck, 2014.

[27] W. Ketterle and N. J. Van Druten, in *Atomic, Molecular, and Optical Physics Volume 37*, edited by B. Bederson and H. Walther (Academic Press, San Diego, 1996), pp. 181–236.

[28] J. Dalibard, Bose- Einstein Condensation in Gases, in *Proceedings of the International School of Physics "Enrico Fermi", Course CXL*, edited by M. Inguscio, S. Stringari, and C. Wieman (IOS Press, Amsterdam, 1999), pp. 321–350.

[29] G. F. Gribakin and V. V. Flambaum, Phys. Rev. A **48**, 546 (1993).

[30] A. A. Golovizin, E. S. Kalganova, D. D. Sukachev, G. A. Vishnyakova, I. A. Semerikov, V. V. Soshenko, D. O. Tregubov, A. V. Akimov, N. N. Kolachevsky, K. Y. Khabarova, and V. N. Sorokin, Quantum Electron. **45**, 482 (2015).

[31] R.-H. Rinkleff and F. Thorn, Z. Phys. D **32**, 173 (1994).

[32] R.-H. Rinkleff, Z. Phys. A **288**, 233 (1978).

[33] X. Chu, A. Dalgarno, and G. C. Groenenboom, Phys. Rev. A **75**, 032723 (2007).

[34] M. Lepers, J.-F. Wyart, and O. Dulieu, Phys. Rev. A **89**, 022505 (2014).

[35] J. Mitroy, M. S. Safronova, and C. W. Clark, J. Phys. B **43**, 202001 (2010).

[36] J. R. P. Angel and P. G. H. Sandars, Proc. R. Soc. London A **305**, 125 (1968).

[37] M. E. Wickliffe and J. E. Lawler, J. Opt. Soc. Am. B **14**, 737 (1997).

[38] H. M. Anderson, E. A. D. Hartog, and J. E. Lawler, J. Opt. Soc. Am. B **13**, 2382 (1996).

[39] R. Cowan, *The Theory of Atomic Structure and Spectra* (University of California Press, Berkeley, CA, 1981), and Cowan programs RCN, RCN2, and RCG.

[40] L. Veseth and H. P. Kelly, Phys. Rev. A **45**, 4621 (1992).

[41] M. F. Gu, Can. J. Phys. **86**, 675 (2008).

[42] S. B. Whitfield, K. Caspary, R. Wehlitz, and M. Martins, J. Phys. B **41**, 015001 (2008).

[43] D. M. Bishop, J. Chem. Phys. **100**, 6535 (1994).

[44] D. Giglberger and S. Penselin, Z. Phys. **199**, 244 (1967).

[45] K. van Leeuwen, E. Eliel, and W. Hogervorst, Phys. Lett. A **78**, 54 (1980).

[46] J. Blaise and P. Camus, Compt. Rend. **260**, 4693 (1965).

[47] T. Middelmann, C. Lisdat, S. Falke, J. S. R. Winfred, F. Riehle, and U. Sterr, IEEE Trans. Instrum. Meas. **60**, 2550 (2011).

[48] T. Rosenband, P. O. Schmidt, D. B. Hume, W. M. Itano, T. M. Fortier, J. E. Stalnaker, K. Kim, S. A. Diddams, J. C. J. Koelemeij, J. C. Bergquist, and D. J. Wineland, Phys. Rev. Lett. **98**, 220801 (2007).

[49] T. Rosenband, D. B. Hume, P. O. Schmidt, C. W. Chou, A. Brusch, L. Lorini, W. H. Oskay, R. E. Drullinger, T. M. Fortier, J. E. Stalnaker, S. A. Diddams, W. C. Swann, N. R. Newbury, W. M. Itano, D. J. Wineland, and J. C. Bergquist, Science **319**, 1808 (2008).

[50] S. Kotochigova and A. Petrov, Phys. Chem. Chem. Phys. **13**, 19165 (2011).

[51] A. de Marchi, G. D. Rovera, and A. Premoli, Metrologia **20**, 37 (1984).

[52] A. Beyer, L. Maisenbacher, K. Khabarova, A. Matveev, R. Pohl, T. Udem, T. W. Hänsch, and N. Kolachevsky, Phys. Scr. **T165**, 014030 (2015).

[53] T. L. Nicholson, S. L. Campbell, R. B. Hutson, G. E. Marti, B. J. Bloom, R. L. McNally, W. Zhang, M. D. Barrett, M. S. Safronova, G. F. Strouse, W. L. Tew, and J. Ye, Nat. Commun. **6**, 6896 (2015).

[54] F. Riehle, *Frequency Standards: Basics and Applications - Fritz Riehle* (Wiley-VCH Verlag GmbH, Weinheim, 2004).

[55] K. Ishikawa, A. Hatakeyama, K. Gosyono-o, S. Wada, Y. Takahashi, and T. Yabuzaki, Phys. Rev. B **56**, 780 (1997).

[56] C. Chin, R. Grimm, P. Julienne, and E. Tiesinga, Rev. Mod. Phys. **82**, 1225 (2010).

[57] N. Kolachevsky, A. Akimov, I. Tolstikhina, K. Chebakov, A. Sokolov, P. Rodionov, S. Kanorski, and V. Sorokin, Appl. Phys. B **89**, 589 (2007).

[58] S. Friebel, C. DAndrea, J. Walz, M. Weitz, and T. W. Hansch, Phys. Rev. A **57**, R20 (1998).

[59] L. D. Landau and E. M. Lifshitz, *Mechanics*, Vol. 1, 3rd ed. (Butterworth-Heinemann, Oxford, 1976).

[60] W. C. Martin, R. Zalubas, and L. Hagan, *Atomic Energy Levels: The Rare-Earth Elements, No. NSRDS-NBS 60* (U.S. Government Printing Office, Washington, D.C., 1978).

[61] V. E. Chernov, D. L. Dorofeev, I. Y. Kretinin, and B. A. Zon, J. Phys. B **38**, 2289 (2005).